Nanoscale

Red phosphorus in its two-dimension limit: novel clathrates with varying band gaps and superior chemical stabilities

Journal:	*Nanoscale*
Manuscript ID	NR-ART-04-2018-002877.R2
Article Type:	Paper
Date Submitted by the Author:	14-Jun-2018
Complete List of Authors:	Zhu, Zhili; Zhengzhou University, School of Physics and Engineering Cui, Ping; University of Science and Technology of China, Hefei National Laboratory for Physical Sciences at the Microscale Cai, Xiao-Lin ; School of Physics and Chemistry, Henan Polytechnic University Xia, Mengjiao; Zhengzhou University Jia, Yu; Zhengzhou University, School of Physics and Engineering Zhang, Shengbai; Rensselaer Polytechnic Institute, Zhang, Zhen-yu; University of Science and Technology of China,

Journal Name

ARTICLE

Red phosphorus in its two-dimension limit: novel clathrates with varying band gaps and superior chemical stabilities

Received 00th March 20xx,
Accepted 00th January 20xx

DOI: 10.1039/x0xx00000x

www.rsc.org/

Zhili Zhu[a,b], Ping Cui[b], Xiaolin Cai[a], Mengjiao Xia[a], Yu Jia*[,a], Shengbai Zhang*[,b,c], and Zhenyu Zhang*[,b]

First-principles calculations within density functional theory reveal the preferred structures of red phosphorus in the two-dimensional (2D) limit to be porous with intriguing structural, electronic, and chemical properties. These few-atomic-layer structures are stabilized as novel 2D clathrates with tunable pore sizes and varying semiconducting band gaps, labelled as V-Hex, P-Monoclinic, P-Hex, and V-Tetr in descending energetic stabilities. The cohesive energies of the 2D clathrates are all substantially higher than that of white phosphorus. More strikingly, the V-Hex structure is energetically as stable as black phosphorene, but possesses distinctly superior chemical stability when exposed to O_2 due to the presence of a much higher activation barrier against chemisorption. We also exploit the salient properties of these 2D clathrates for their important application potentials, including serving as effective elemental photocatalysts for visible-light-driven water splitting, and as a new class of sieves for molecular separation and DNA sequencing.

1. Introduction

Since the mechanical exfoliation of graphene from graphite in 2004, [1] exploration of other types of two-dimensional (2D) materials has attracted tremendous research interest.[2-13] Centered on the fabrication of 2D materials is the existence of layered materials from which the 2D materials can be obtained straightforwardly by exfoliation, although other approaches such as epitaxial growth also became available. Taking phosphorus as an example, which has a number of allotropes such as the white, black, red and violet phosphorus, [14, 15] one can make black phosphorene (α-P) by an exfoliation of black phosphorus.[7] Another interesting phosphorene is the blue phosphorene (β-P) which does not have corresponding bulk layered material, but a fourfold-coordinated A7 phase instead. [9, 16] In addition to the black and blue phosphorenes, many other 2D allotropes of phosphorus have been proposed[17-20]. However, all these previously predicted allotropes have been made by invoking subunits of phosphorus clusters smaller than P6.The β-P was first predicated by first-principles calculations and subsequently fabricated by experiment,[21] which raises an important question that has not been fully appreciated by the community: namely, can one fabricate 2D materials when the corresponding layered structure does not exist?

A definitive answer to the above question could potentially open a different route for fabricating a large number of 2D materials of unexpected form and properties. Indeed, recent experimental and theoretical study of tellurium is a solid example that one could obtain 2D tellurenes whose bulk structure is a quasi-1D solid with helical chains. [13] Another example is the traditional semiconductors in their 2D limit, which have been predicted to show a double honeycomb structure. [22] If we follow this line of thought and revisit the phosphorus allotropes, the Hittorf's red phosphors[23] with a tubular quasi 1D structure would be potentially interesting. Recently, Liu *et al.*[24] predicted a 1D chain of phosphorus structurally closely resembles the red phosphorus, which has subsequently been claimed to be experimentally verified. [25] A double-layer 2D structure for Hittorf's phosphorus was proposed by Schusteritsch *et al.*,[26] which consists of connected 1D chains of P and expected to have a large direct band gap and high mobility.

Here we predict the existence of previously unknown phosphorenes, as the 2D limits of red phosphorus, possessing salient structural, electronic, and chemical properties. Our density functional theory (DFT) calculations identify four different types of the 2D phosphorenes, labeled as V-Hex, P-Monoclinic, P-Hex, and V-Tetr, all of which are stabilized as novel 2D clathrate lattices with variable pore sizes. Although none of the structures here has the corresponding layered

[a] International Laboratory for Quantum Functional Materials of Henan, and School of Physics and Engineering, Zhengzhou University, Zhengzhou 450001, China. E-mail: jiayu@zzu.edu.cn
[b] International Center for Quantum Design of Functional Materials (ICQD), Hefei National Laboratory for Physical Sciences at the Microscale, and Synergetic Innovation Center of Quantum Information and Quantum Physics, University of Science and Technology of China, Hefei, Anhui 230026, China. E-mial: zhangzy@ustc.edu.cn
[c] Department of Physics, Applied Physics, & Astronomy, Rensselaer Polytechnic Institute, Troy, New York 12180, USA. E-mail : zhangs9@rpi.edu

bulk, their formation energies are surprisingly low. In particular, V-Hex is as stable as α-P and is considerably more stable than β-P. In other words, this is the first known example of a 2D structure lack of layered bulk but with an energy as stable as the one from exfoliation.

These 2D clathrates also possess distinctly superior chemical stabilities when exposed to O_2, as evidenced by the presence of a much larger activation barrier against chemisorption than that of α-P. It enables their salient properties to be exploited for important technological applications. As one compelling example, the band gaps of P-Monoclinic, P-Hex, and V-Tetr of 1.90 to 2.36 eV straddle both the H^+/H_2 and O_2/H_2O levels, pointing to their potentials as efficient elemental photocatalysts for water splitting. The V-Hex, on the other hand, offers a highly appealing application as sieves for molecular separation and DNA sequencing, enabled by the tunable pore sizes from 1 to 4 nm.

2. Methods

All calculations were performed with DFT calculations using the Vienna ab initio simulation package (VASP) within the projector augmented wave method.[27, 28] For the exchange-correlation energy, we employed the Perdew-Burke-Ernzerhof (PBE) functional[29] and the Heyd, Scuseria, and Ernzerhof (HSE06) [30, 31] screened hybrid functional in obtaining the electronic structures. The kinetic energy cutoff for the plane wave basis set was chosen to be 400 eV. The 2D monolayers were modelled with periodic slab geometry and a vacuum thickness of 20 Å to avoid possible effects of image supercells. All the atoms in the supercell were allowed to be fully relaxed until the Hellmann-Feynman forces are less than 0.01 eV/Å. The Brillouin zone was sampled using 5×5×1 and 7×7×1 Monkhorst-Pack k-point meshes for large (>15 Å) and small (<11 Å) supercells, respectively. The 2×2 (>15 Å) and 3×3 (<11 Å) supercells were adopted to perform phonon calculations by using Phonopy, as implemented in the VASP code. [32] When studying the adsorption and dissociation of oxygen molecules, we employ the van der Waals (vdW) correction proposed by Grimme[33]. Spin polarization is also explicitly included.

3. Results and discussion

3.1 Construction rules and geometric structures of clathrate phosphorenes

Red phosphorus[23] has a distinct monoclinic structure (space group P2/c) made by phosphorus clusters, known as the P_8 and P_9 building units. The blocks are linked together by phosphorus pairs (P_2) in an alternating P_8/P_9 fashion to form tubes with a pentagonal cross section. It is the P_9 units that connect the tubes together to form the 3D structure. The internal tubular structure of red phosphorus has prompted the prediction of quasi-1D ring-shaped and helically-coiled structures made of P_8 and P_2 units.[25, 34] While a stable molecular precursor for the main building unit of the 1D structure P_8 has yet to be experimentally demonstrated, quasi-1D ring-shaped phosphorus can be obtained by sublimating red phosphorus at elevated temperatures. [25]

To fabricate new 2D structures of red phosphorus, we first identify which kind of phosphorus clusters as the building block. Here, the P_{12} are used based on its higher geometric symmetry than P_{10} and P_{14}, which the simple and intriguing 2D structures may be expected. Of course, the other phosphorus clusters also can be used as the building blocks to construct more complex 2D structures. Fig. 1(a) shows a hydrogen-terminated P_{12}. Unlike P_8, stable molecular precursors for P_{12} exist, for example as $P_{12}Me_4$, $P_{12}Et_4$, and $P_{12}Pr^i_4$. [35] Hence, it is highly possible that, besides the sublimation approach, one should be able to obtain the stable forms of the 2D red phosphorus by self-assembly similar to the fabrication of graphene nanowiggles.[36]

Before diving into the structural details of the 2D red phosphorus, it can be constructive to first consider the hydrogenation of $P_{12}H_4$ in all possible configurations. As shown in Fig. S1, according to the relative orientations of the four hydrogen atoms of both sides in $P_{12}H_4$, five possible structures can be constructed. Fig. 1(a) is the one with lowest energy, where the optimal bond angles are $\angle HP_1P_2$ = 95.8° and $\angle HP_1P_3$ = 92.8°. The other four are given in Fig.S1 (b)-(e), respectively, in the Supplementary Materials. It is found that the preferred hydrogen bonding directions do not favor the quasi-1D structures as the P_8 does. Instead, they all favor 2D structures.

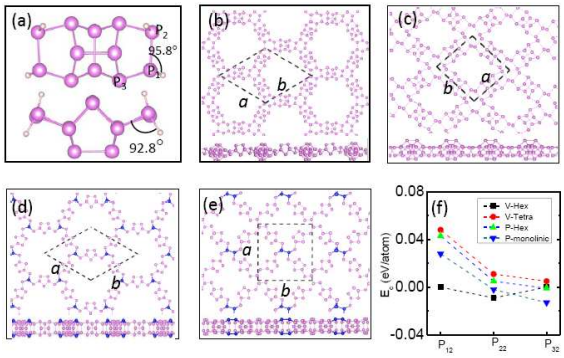

Fig. 1 Top and side views of subunit and optimized structures of clathrate phosphorenes for (a) $P_{12}H_4$, (b) P-Hex, (c) P-Monoclinic, (d) V-Hex, (e) V-Tetr. The dashed lines denote the shapes (black) of the unit cells. (f) Cohesive energy per atom (E_c) relative to black phosphorene for different 2D clathrates formed with P_{12}, P_{22} and P_{32} subunits. The bridge P atoms and P dimers between P_{12} blocks in (d) and (e) are highlighted in blue.

In a P_{12} unit, each P atom has a p^3- (also known as an s^2p^3-) electronic hybridization with two electrons in a lone-pair orbital, while the other three are shared by neighboring atoms to form three σ-bonds. When P_{12} units assemble, an end P atom only bonded with two neighboring P atoms prefers to form a third covalent bond, thereby potentially resulting in 2D structures. We define two different types of candidate 2D structures: parallel, labelled as "P-", in which the planner orientation of the P_{12} units coincides with that of the 2D networks; and vertical, labelled as "V-", in which the planner orientation of the P_{12} units is perpendicular to that of the 2D

networks. Such construction rules lead to the identification of only four different allotropes, labelled as P-Hex, P-Monoclinic, V-Hex, and V-Tetr. The structural parameters and physical properties of the optimized allotropes are listed in Table 1, with more details presented in the following discussions. Intriguingly, such 2D allotropes possess novel 2D clathrates with different pore sizes.

Table 1 Structural and physical properties of clathrate phosphorenes. a and b are the superlattice constants. E_c is the cohesive energy per atom relative to black phosphorene. n denotes the total number of atoms in the unit cell.

structure	P-Hex	P- Monoclinic	V-Hex	V-Tetr
$\|a\|$ (Å)	17.07	10.06	16.83	15.87
$\|b\|$ (Å)	17.07	10.84	16.83	15.87
E_c (eV/atom)	0.04	0.03	0	0.05
n	36	24	40	56

First, we discuss the P-Hex and P-Monoclinic structures shown in Figs. 1(b) and (c), respectively. The P-Hex allotrope possesses a buckled honeycomb structure with the superlattice constant of a = 17.07 Å and the pore diameter of ~13 Å. There are three P_{12} blocks in the unit cell, and the six end atoms bond together to form a slightly buckled hexamer similar to that of blue phosphorene.9 In this regard, the P-Hex allotrope can also be viewed as three P_8 units linked by a commonly shared hexamer node [See Fig. S2 (a)]. In contrast, the P-Monoclinic allotrope has a monoclinic structure with superlattice constants of a = 10.06 Å and b = 10.84 Å, and the angle between the *a* and *b* axes is 84.4°. In this structure, four P_{12} units are arranged in the unit cell, and the angle between adjacent blocks is close to 90°. The eight end atoms from the four P_{12} units bond together, forming a highly buckled octamer with ∠PPP angles of 108.4° and 104.7° [see Fig. S2 (b)]. The pore size of the P-Monoclinic allotrope is ~7 Å.

Next we move to the case of V-Hex, and V-Tetr. Here, due to the bond direction constraints, extra P atoms or P dimers are needed to bridge two neighboring P_{12} units, leading to the two distinctly different structures of V-Hex and V-Tetr shown in Figs. 1(d) and (e), respectively. For the V-Hex structure, three P_{12} units in the unit cell are arranged with a common angle of 120° and linked together by two extra P atoms (one above and one below the central plane of the 2D structure as highlighted in blue), forming a large hexagonal superlattice with a = 16.83 Å. The pore diameter of the V-Hex allotrope is ~14 Å. The ∠ PPP angles between the upper and lower extra P atoms and the P_{12} units are 106.56° and 101.04° respectively [See Fig. S2(c)]. For the V-Tetr allotrope, four P_{12} units in the unit cell are connected by two extra P_2 dimers (again one above and one below the central plane of the 2D structure as highlighted in blue). The V-Tetr allotrope has a square structure with a superlattice constant of a = 15.87 Å, forming a square 2D clathrate lattice with pore size ~8 Å. The upper and lower dimers connect the P_{12} units with linking angles of 105.78° and 98.02°, respectively [See Fig. S2 (d)].

The vdW effects on the structure and stability of these 2D systems have been checked. It was found that the optimized lattice parameters exhibit slight variations when the vdW corrections are included. However, the relative stabilities of the various allotropes remain unchanged.

3.2 Stability of clathrate phosphorenes

Now, we examine the relative energetic stability of different 2D clathrates discussed above, measured by the cohesive energy (E_c) per atom, with that of black phosphorene as the reference. The results are summarized in Table 1, showing that each of the four 2D clathrate is substantially more stable than white phosphorus. The cohesive energy differences between these clathrates and black phosphorene are also less than 0.05 eV/atom, while the difference is ~0.16 eV/atom between white and black phosphorus. In particular, the stable V-Hex allotrope has essentially the same cohesive energy as black phosphorene. To gain further insights of the stability of these 2D clathrates, we also compared their total energies with that of infinite 1D chains made of the P_{10} units. It was found that the isolated 1D chains are energetically as stable as the black phosphorene. As such, the relative energies of the clathrates are almost the same as those calculated when the black phosphorene is used as the reference. Additionally, as presented in Fig. 2, our phonon spectrum calculations indicate that each of the four 2D clathrates is dynamically stable. It shows a small imaginary phonon mode near the Γ point in the P-Monoclinic structure. It will disappear through the phonon calculation with increased supercell size, which reflects a typical problem of 2D syatems.[37] These stability analyses help to enhance the feasibility of experimentally fabricating such structures. The dynamic stability was further investigated using *ab initio* molecular dynamics (MD) simulations at finite temperatures. It was found that the equilibrium structures of the 2D clathrates are stable at the room temperature. In the movies of the Supplementary, we illustrate the dynamic stability of the 2D clathrates at 300 K up to a time period of 3 ps with 1 fs time step.

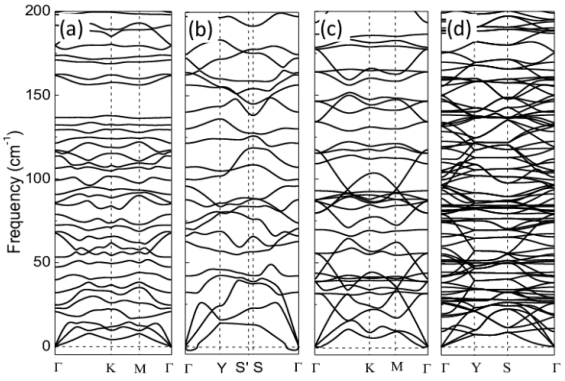

Fig. 2 Phonon spectra of the clathrate phosphorenes of (a) P-Hex, (b) P-Monoclinic, (c) V-Hex, and (d) V-Tetr. For clarity, the frequencies are shown within 200 cm^{-1}.

Another critically important aspect to examine is the chemical stability of these predicted clathrate phosphorenes,

especially given the observation that black phosphorene can be easily oxidized when exposed to oxygen.[38, 39] The underlying mechanism was revealed in a recent theoretical study, showing that an O_2 molecule experiences only a low potential energy barrier of 0.54 eV from physisorption to chemisorption on black phosphorene.[40] It is therefore worthwhile to evaluate the stability of these 2D clathrates in the presence of O_2 molecules, which are abundant in air and other technologically relevant environments.

Without loss of generality, here we discuss the O_2 adsorption and dissociation processes on the stable V-Hex clathrate. Different P atomic positions in the nanopore are considered as potential adsorption sites. While the results are given in Fig. S3, Fig. 3 (a) shows the result for the most-stable adsorption. As an O_2 molecule approaches the V-Hex, it will first reach a locally stable adsorption configuration as shown in Fig. 3(a), where the O_2 molecule adsorbs on the two bonded P atoms in the center of the P_{12} unit. The corresponding adsorption energy is only ~0.06 eV, while the distance between O_2 and the P-P pair is 3.3 Å, indicating that the O_2 molecule is physisorbed on V-Hex. When the O_2 further approaches the P-P pair, the total energy first increases to 1.64 eV. At the transition state (TS), the distance between the center of the O_2 and that of the P-P pair is ~1.96 Å. Once the O_2 passes the TS, the total energy starts to decrease as a result of the O2 dissociation. At the final state (FS), the equilibrium O-P bond lengths are ~1.49 Å and the adsorption energy is 4.52 eV. The potential energy barrier between the IS and FS is as high as 1.64 eV as shown in Fig. 3(d), indicating that the V-Hex clathrate phosphorene possesses much higher chemical stability upon O_2 adsorption than black phosphorene. The superior chemical stability is further quantified by *ab initio* MD simulations. In the movie of the Supplementary, we present the dynamic stability of V-Hex exposed to O_2 at 300 K up to a time period of 6 ps with 1 fs time step.

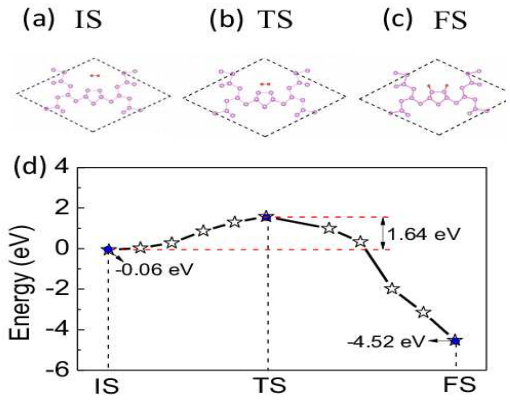

Fig. 3 Top views of optimized structures for the adsorption and dissociation processes of O_2 molecule on the V-Hex clathrate, highlighting only the area within a unit cell. (a) Initial State (IS), defined by the physisorbed configuration; (b) Transition S State (TS); (c) Final State (FS), characterized by dissociative chemisorption. (d) Energy profile of O_2 adsorption and dissociation on the V-Hex clathrate. The P and O atoms are colored in pink and red, respectively.

Electronic and optical properties of clathrate phosphorenes.

The electronic properties of such new clathrate phosphorenes are characterized by their band structures. The results within the PBE functional scheme are shown in Fig. S4, indicating that all these 2D allotropes exhibit semiconducting characters. The P-Monoclinic and V-Tetr allotropes are semiconductors with direct band gaps of E_g = 1.19 and 1.64 eV, respectively; in contrast, the P-Hex and V-Hex allotropes are semiconductors with indirect band gaps of E_g = 1.57 and 1.89 eV respectively. Since the PBE scheme may underestimate the band gaps, we have also performed hybrid DFT calculations within the HSE06 functional, given by 2.35, 1.90, 2.72, and 2.36 eV for P-Hex, P-Monoclinic, V-Hex, and V-Tetr, respectively, as shown in Fig. 4. The carrier mobilities of such 2D clathrates were also estimated as exemplified by the stable V-Hex. The calculated effective masses are m^*_e = 0.57 m_e, and m^*_h = 0.69 m_e. Using the acoustic phonon limited method, [41] the electron and hole mobilities are calculated to be 160 and 1700 $cm^2 V^{-1} s^{-1}$, which are comparable to those reported for a double-layer, non-clathrate 2D structure by Hittorfene.[26]

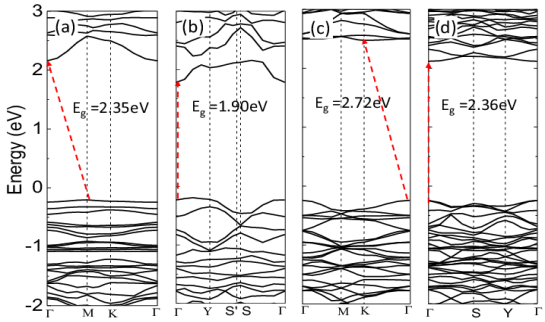

Fig. 4 Band structures of the clathrate phosphorenes obtained within the HSE06 scheme for (a) P-Hex, (b) P-Monoclinic, (c) V-Hex, and (d) V-Tetr, all based on the P_{12} building units.

We have also investigated the optical absorption spectra of these 2D clathrates, given by the imaginary parts of the frequency-dependent dielectric functions within the HSE06 scheme. The results are shown in Fig. 5, indicating that relatively higher absorption is expected for the two clathrate phosphorenes with direct band gaps than the other two with indirect band gaps.

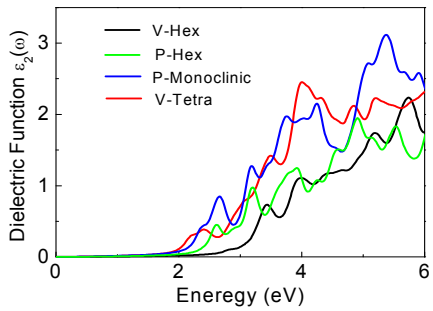

Fig. 5 Imaginary part of the dielectric function for the four clathrate phosphorenes.

3.3 Tunable pore sizes of clathrate phosphorenes

So far we have limited to 2D clathrates based on the P_{12} units. When other phosphorus clusters are considered as building blocks, a wide range of additional candidate allotropes may also emerge. In the present study, we still limit ourselves to building blocks corresponding to segments of Hittorf's red phosphorus with different lengths. We therefore adopt P_{22} or P_{32} clusters as building blocks to construct clathrate phosphorenes in the same geometries of P-Hex, P-Monoclinic, V-Hex, and V-Tetr but with approximately doubled or tripled side lengths of the nanopores. The optimized geometric structures of the 2D allotropes formed with the P_{22} and P_{32} units are shown in Fig. S5. The cohesive energies of the four structures using the P_{12}, P_{22}, and P_{32} uints are presented in Fig. 1(f), indicating that all the four types of structures using the two larger building blocks can be energetically as stable as black phosphorene. The energetic stabilities of the 2D clathrates are dominated by the covalent interatomic bonds of both the inner- and inter-units. Compared with an infinite 1D chain, there exist small distortions at where the units join. As the units get larger, the portion with distortion decreases whereby the total energy is lowered.

3.4 Potential applications of clathrate phosphorenes

The various salient properties of these 2D clathrates revealed above are expected to find diverse technological applications. As the first compelling example, here we study the photocatalytic properties of these 2D structures. Recently, red phosphorus has been demonstrated to be a promising candidate photocatalyst for solar to chemical energy conversion owing to its absorbance of long wavelength photons up to 700 nm (corresponding to a 1.8 eV band gap) and its ability to split water under visible light irradiation. [42, 43] Compared to bulk red phosphorus, the photocatalytic activity of the clathrate phosphorenes is likely to be substantially improved if these materials are also suitable for photocatalysis, due to their ultrathin thickness and large specific surface area with highly accessible active sites. Indeed, the calculated specific surface areas for the proposed 2D allotropes can reach up to ~2.7×10^3 m^2/g, much higher than that of micron-sized red phosphorus particles typically used in previous studies.

In exploring their photocatalytic activity, we first note that the band gaps of P-Hex, P-Monoclinic, and V-Tetr satisfy the desirable gap criteria for efficient water splitting, [44] while the band gap of the stable V-Hex is too large for efficient solar energy absorption. In addition, the work functions of the three relevant structures are calculated to be 5.83 eV (V-Tetr), 6.00 eV (P-Hex), and 5.71 eV (P-Monoclinic), which are all comparable with the standard oxidation potential of O_2/H_2O (−5.67 eV) [45] and reduction potential of H^+/H_2 (−4.44 eV). Figure 6 shows the band alignment of the clathrate phosphorenes calculated within the HSE06 scheme, together with the chemical reaction potentials for H^+/H_2 and O_2/H_2O. Indeed, the hydrogen reduction potential and oxygen oxidation potential are located within the band gaps of the three systems, which are therefore promising candidate photocatalysts for practical applications in visible-light-driven water splitting.

Another apparent and highly appealing potential application is for chemical and biological sensing and separation, due to the relatively large and tunable pore sizes of the clathrate phosphorenes. As potential molecular targets, the P_{12}-based V-Hex allotrope has the suitable pore size for detection of nicotine, [46] while the P_{22}-based V-Hex allotrope has the pore size of ~25 Å, ideally satisfying the requirement of the nanopore diameter of at least 2.3 nm for the translocation of dsDNA.[47] Compared with the existing approach of DNA sequencing by e-beam drilling, here we completely eliminate the damage by the electron beam. We have examined the stability of the V-Hex allotrope in water since biological macromolecules usually exist in a solution. Our DFT calculations show that H_2O molecules can only physisorb on the V-Hex allotrope, with the largest adsorption energy being 0.145 eV (see Fig. S6). Therefore, the V-Hex allotrope is stable in water, in fact even in the presence of visible light. Detailed systemic investigation of the interaction of DNA with the V-Hex clathrate phosphorene is an ongoing research effort.

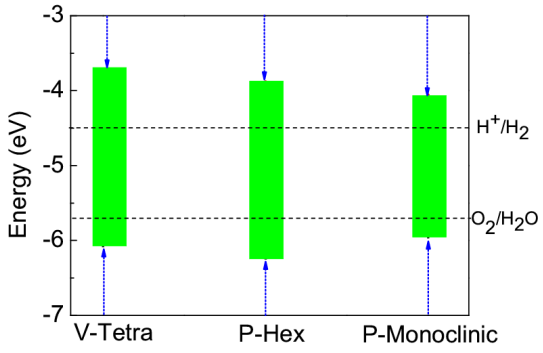

Fig. 6 Band alignments of the three clathrate phosphorenes calculated within the HSE06 scheme. The vacuum level is set to be 0 eV. The dashed lines denote the chemical reaction potentials for H^+/H_2 and O_2/H_2O, respectively. The vertical bars in green denote the band gaps.

4. Conclusions

In conclusion, we showed that 2D forms of red phosphorus indeed exist and are exceptionally stable. We further showed that these 2D structures are 2D clathrates with periodic pore structures of various shapes and sizes. As importantly, they all possess distinct structural, electronic, and chemical properties. Unlike α-P, these 2D clathrates also possess distinctly superior chemical stability when exposed to O_2 as measured by the > 1.5 eV activation barrier against dissociation and chemisorption. Among the four types of structures that we have found, three may serve as effective elemental photocatalysts for water splitting, while the other should

provide a new and much more desirable platform for DNA sequencing. Last but not least, molecular precursors exist in the lab that makes the self-assembly of 2D clathrates also experimentally feasible.

Conflicts of interest

There are no conflicts to declare.

Acknowledgements

This work was partially supported by the NSFC (No. 11634011, 11722435, 11504357, 61434002, and 11774078), the NSF of Henan Province of China (No.162300410254), and the National Key Basic Research Program of China (Grant No. 2017YF0303500). S.B.Z. was supported by the NSF Grant No. DMREF-1626967. The calculations were performed on the High Performance Clusters of Zhengzhou University.

Notes and references

1. K. S. Novoselov, A. K. Geim, S. V. Morozov, D. Jiang, Y. Zhang, S. V. Dubonos, I. V. Grigorieva and A. A. Firsov, *Science*, 2004, **306**, 666-669.
2. A. J. Mannix, X. F. Zhou, B. Kiraly, J. D. Wood, D. Alducin, B. D. Myers, X. Liu, B. L. Fisher, U. Santiago and J. R. Guest, *Science*, 2015, **350**, 1513.
3. B. Feng, J. Zhang, Q. Zhong, W. Li, S. Li, H. Li, P. Cheng, S. Meng, L. Chen and K. Wu, *Nat Chem*, 2016, **8**, 563-568.
4. P. Vogt, P. De Padova, C. Quaresima, J. Avila, E. Frantzeskakis, M. C. Asensio, A. Resta, B. Ealet and G. Le Lay, *Phys. Rev. Lett.*, 2012, **108**, 155501.
5. M. E. Dávila, L. Xian, S. Cahangirov, A. Rubio and G. Le Lay, *New Journal of Physics*, 2014, **16**, 095002.
6. F.-f. Zhu, W.-j. Chen, Y. Xu, C.-l. Gao, D.-d. Guan, C.-h. Liu, D. Qian, S.-C. Zhang and J.-f. Jia, *Nat Mater*, 2015, **14**, 1020-1025.
7. L. Li, Y. Yu, G. J. Ye, Q. Ge, X. Ou, H. Wu, D. Feng, X. H. Chen and Y. Zhang, *Nature Nanotechnology*, 2014, **9**, 372.
8. H. Liu, A. T. Neal, Z. Zhu, Z. Luo, X. Xu, D. Tománek and P. D. Ye, *ACS Nano*, 2014, **8**, 4033-4041.
9. Z. Zhu and D. Tománek, *Phys. Rev. Lett.*, 2014, **112**, 176802.
10. J. Zeng, P. Cui and Z. Zhang, *Phys. Rev. Lett.*, 2017, **118**, 046101.
11. J. Ji, X. Song, J. Liu, Z. Yan, C. Huo, S. Zhang, M. Su, L. Liao, W. Wang, Z. Ni, Y. Hao and H. Zeng, *Nature Communications*, 2016, **7**, 13352.
12. F. Reis, G. Li, L. Dudy, M. Bauernfeind, S. Glass, W. Hanke, R. Thomale, J. Schäfer and R. Claessen, *Science*, 2017, **357**, págs. 287-290.
13. Z. Zhu, X. Cai, S. Yi, J. Chen, Y. Dai, C. Niu, Z. Guo, M. Xie, F. Liu, J. H. Cho, Y. Jia and Z. Zhang, *Phys. Rev. Lett.*, 2017, **119**, 106101.
14. R. Hultgren, N. S. Gingrich and B. E. Warren, *J. Chem. Phys.*, 1935, **3**, 351-355.
15. H. Thurn and H. Kerbs, *Angew. Chem. Int. Ed.*, 2010, **5**, 1047-1048.
16. S. E. Boulfelfel, G. Seifert, Y. Grin and S. Leoni, *Physical Review B*, 2012, **85**, 014110.
17. J. Guan, Z. Zhu and D. Tomanek, *Phys. Rev. Lett.*, 2014, **113**, 046804.
18. M. Wu, H. Fu, L. Zhou, K. Yao and X. C. Zeng, *Nano Lett.*, 2015, **15**, 3557-3562.
19. Z. Zhuo, X. Wu and J. Yang, *J. Am. Chem. Soc.*, 2016, **138**, 7091-7098.
20. J. Guan, Z. Zhu and D. Tománek, *Acs Nano*, 2014, **8**, 12763-12768.
21. J.-P. Xu, J.-Q. Zhang, H. Tian, H. Xu, W. Ho and M. Xie, *Physical Review Materials*, 2017, **1**, 061002.
22. M. C. Lucking, W. Xie, D.-H. Choe, D. West, T.-M. Lu and S. B. Zhang, *Phys. Rev. Lett.*, 2018, **120**, 086101.
23. H. K. V. H. Thurn, *Acta Crystallogr.*, 1969, **B25**, 125-135.
24. D. Liu, J. Guan, J. Jiang and D. Tomanek, *Nano Lett.*, 2016, **16**, 7865-7869.
25. J. Zhang, D. Zhao, D. Xiao, C. Ma, H. Du, X. Li, L. Zhang, J. Huang, H. Huang, C. L. Jia, D. Tomanek and C. Niu, *Angew. Chem. Int. Ed. Engl.*, 2017, **56**, 1850-1854.
26. G. Schusteritsch, M. Uhrin and C. J. Pickard, *Nano Lett.*, 2016, **16**, 2975-2980.
27. G. Kresse and J. Hafner, *Physical Review B*, 1993, **48**, 13115.
28. G. Kresse and J. Furthmüller, *Computational Materials Science*, 1996, **6**, 15-50.
29. J. P. Perdew, K. Burke and M. Ernzerhof, *Phys. Rev. Lett.*, 1996, **77**, 3865.
30. J. Heyd, G. E. Scuseria and M. Ernzerhof, *The Journal of Chemical Physics*, 2003, **118**, 8207-8215.
31. A. V. Krukau, O. A. Vydrov, A. F. Izmaylov and G. E. Scuseria, *J. Chem. Phys.*, 2006, **125**, 224106.
32. A. Togo, F. Oba and I. Tanaka, *Physical Review B*, 2008, **78**, 134106.
33. S. Grimme, *J. Comput. Chem.*, 2006, **27**, 1787-1799.
34. A. J. Karttunen, M. Linnolahti and T. A. Pakkanen, *Chemistry*, 2007, **13**, 5232-5237.
35. M. Baudler and K. Glinka, *Monocyclic and polycyclic phosphanes*1993.
36. R. A. Bizao, T. Botari, E. Perim, N. M. Pugno and D. S. Galvao, *Carbon*, 2017, **119**, 431-437.
37. H. Zheng, X.-B. Li, N.-K. Chen, S.-Y. Xie, W. Q. Tian, Y. Chen, H. Xia, S. Zhang and H.-B. Sun, *Physical Review B*, 2015, **92**, 115307.
38. J. Kang, J. D. Wood, S. A. Wells, J. H. Lee, X. Liu, K. S. Chen and M. C. Hersam, *Acs Nano*, 2015, **9**, 3596-3604.
39. M. Serrano‐Ruiz, M. Caporali, A. Ienco, V. Piazza, S. Heun and M. Peruzzini, *Advanced Materials Interfaces*, 2016, **3**, 1500441.
40. A. Ziletti, A. Carvalho, D. K. Campbell, D. F. Coker and A. H. Castro Neto, *Phys. Rev. Lett.*, 2015, **114**, 046801.
41. J. Qiao, X. Kong, Z.-X. Hu, F. Yang and W. Ji, *Nature Communications*, 2014, **5**, 4475.
42. G. Liu, P. Niu and H. M. Cheng, *Chemphyschem A European Journal of Chemical Physics & Physical Chemistry*, 2013, **14**, 885.
43. F. Wang, W. K. H. Ng, J. C. Yu, H. Zhu, C. Li, L. Zhang, Z. Liu and Q. Li, *Applied Catalysis B Environmental*, 2012, **111**, 409-414.
44. M. G. Walter, E. L. Warren, J. R. Mckone, S. W. Boettcher, Q. Mi, E. A. Santori and N. S. Lewis, *Chem. Rev.*, 2010, **110**, 6446.

45. V. Chakrapani, J. C. Angus, A. B. Anderson, S. D. Wolter, B. R. Stoner and G. U. Sumanasekera, *Science*, 2007, **318**, 1424.
46. S. J. Ray, *J. Appl. Phys.*, 2014, **116**, 29-185.
47. C. Sathe, X. Zou, J. P. Leburton and K. Schulten, *Acs Nano*, 2011, **5**, 8842-8851.